



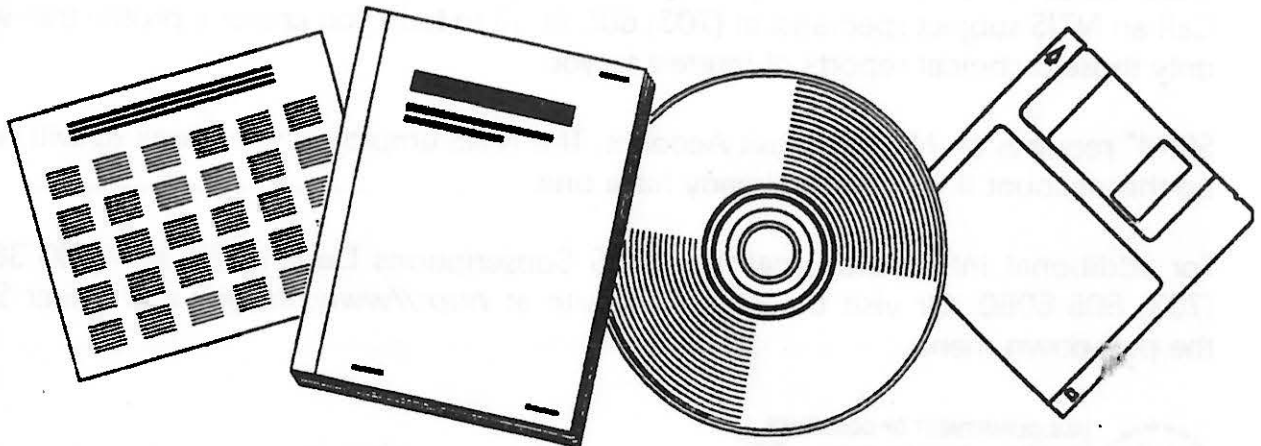
DE82006998

NTIS[®]
Information is our business.

CONTACT STRESSES ON A THIN PLATE AFTER LARGE DISPLACEMENTS TO A HALF PARABOLIC SURFACE

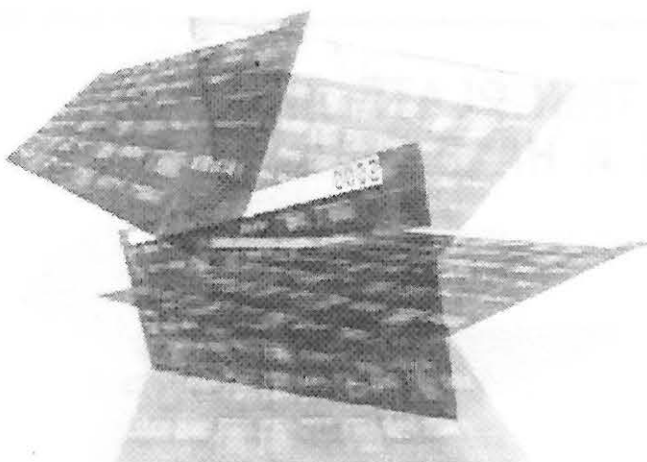
SANDIA NATIONAL LABS.
ALBUQUERQUE, NM

JAN 1982



U.S. DEPARTMENT OF COMMERCE
National Technical Information Service

Tailored to Your Needs!



Selected Research In Microfiche

SRIM® is a tailored information service that delivers complete microfiche copies of government publications based on your needs, automatically, within a few weeks of announcement by NTIS.

SRIM® Saves You Time, Money, and Space!

Automatically, every two weeks, your SRIM® profile is run against all *new* publications received by NTIS and the publications microfiched for your order. Instead of paying approximately \$15-30 for each publication, you pay only \$2.50 for the microfiche version. Corporate and special libraries love the space-saving convenience of microfiche.

NTIS offers two options for SRIM® selection criteria:

Standard SRIM®—Choose from among 350 pre-chosen subject topics.

Custom SRIM®—For a one-time additional fee, an NTIS analyst can help you develop a keyword strategy to design your Custom SRIM® requirements. Custom SRIM® allows your SRIM® selection to be based upon *specific subject keywords*, not just broad subject topics. Call an NTIS subject specialist at (703) 605-6655 to help you create a profile that will retrieve only those technical reports of interest to you.

SRIM® requires an NTIS Deposit Account. The NTIS employee you speak to will help you set up this account if you don't already have one.

For additional information, call the NTIS Subscriptions Department at 1-800-363-2068 or (703) 605-6060. Or visit the NTIS Web site at <http://www.ntis.gov> and select SRIM® from the pull-down menu.



U.S. DEPARTMENT OF COMMERCE
Technology Administration
National Technical Information Service
Springfield, VA 22161 (703) 605-6000
<http://www.ntis.gov>

CONTACT STRESSES ON A THIN PLATE AFTER LARGE
DISPLACEMENTS TO A HALF PARABOLIC SURFACE*

Rodney K. Wilson
Robert C. Reuter, Jr.
Sandia National Laboratories
Albuquerque, NM 87185

Abstract

In a previous report a solution was obtained for the determination of all loads necessary to hold an initially flat, thin, elastic plate in the shape of a prescribed parabolic surface, following large displacement. These loads include spatially varying normal tractions distributed over the back surface of the plate, and a uniform shear force and bending moment applied along the opposing edges which become the rims of the parabola after deformation. In actual practice the edge loads are not present and, as a result, local displacement and stress variations arise creating what is known as an edge effect. Furthermore, if the full parabola is separated into two equal halves at the vertex another edge effect occurs. The analysis used to compute the local displacement and stress variations arising near the rim is repeated here to treat the absence of edge loads at the vertex. In addition to the normal stresses which arise, shear stresses result from the absence of the membrane reaction at the vertex, which was present in the case of the full parabolic surface. Correlation between the present theory and data from laser ray trace experiments is also presented.

*This work performed at Sandia National Laboratories supported by the U.S. Department of Energy under contract number DE-AC04-76DP00789.

TABLE OF CONTENTS

| | <u>Page</u> |
|--------------------------------|-------------|
| Nomenclature | 6 |
| Introduction | 7 |
| Analysis | 7 |
| Discussion of Results. | 23 |
| References | 27 |

ILLUSTRATIONS

| | |
|--|----|
| 1. Assembled, parabolic, line focusing solar collector. . . | 8 |
| 2. Diagram of half of the deformed, reflective surface explicating coordinates, rim and vertex loads and pressure distribution required to achieve the true parabolic shape. | 9 |
| 3. Contact stresses in adhesive applied to backside of deformed reflective surface arising from edge effect at rim | 12 |
| 4. Rotation of surface normals (slope error) arising from edge effect at rim | 13 |
| 5. Diagram of the flat-plate model of the edge effect region at vertex explicating the coordinate system and semi-infinite extension. | 15 |
| 6. Contact stresses in adhesive applied to backside of deformed reflective surface arising from edge effect at vertex. | 8 |
| 7. Rotation of surface normals (slope error) arising from edge effect at vertex | 17 |
| 8. Diagram of the flat plate model used to analyze shear deformation arising from edge effect at vertex | 20 |
| 9. Shear stresses in adhesive applied to backside of deformed reflective surface arising from edge effect at vertex. | 22 |

| | |
|--|----|
| 10. Typical results from laser ray tracing showing slope errors at rim and vertex | 24 |
| 11. Single scan taken from laser ray tracing showing slope errors at rim and vertex | 25 |
| 12. Correlation between analytical results [eqs (7) and (13)] and laser ray tracing data (Fig. 11) | 26 |

NOMENCLATURE

| | |
|---------------|---|
| D | flexural rigidity of reflective surface |
| E_p | Young's modulus of reflective panel |
| f | focal length of parabola |
| h_a | thickness of adhesive |
| G_a | shear modulus of adhesive |
| h_p | thickness of reflective panel |
| k | stiffness of adhesive plus substructure |
| M_R | bending moment applied at rim to maintain true parabolic shape |
| M_V | bending moment applied at vertex to maintain true parabolic shape |
| N_V | membrane load at vertex to maintain true parabolic shape |
| P_C | contact pressure applied over back surface of reflective panel to maintain true parabolic shape |
| Q_R | shear force applied at rim to maintain true parabolic shape |
| $w_R(x)$ | displacement of reflective surface at x due to edge effect at rim |
| $w_V(x)$ | displacement of reflective surface at x due to edge effect at vertex |
| x, y | rectangular coordinates |
| β | panel-adhesive-substructure stiffness parameter |
| γ | panel-adhesive shear parameter |
| δ_2 | second cross-over distance |
| ν | Poisson's ratio |
| $\sigma_R(x)$ | normal contact stress at x due to edge effect at rim |
| $\sigma_V(x)$ | normal contact stress at x due to edge effect at vertex |
| $\tau(x)$ | shear contact stress at x due to edge effect at vertex |

INTRODUCTION

A current line focusing solar collector design involves bonding two initially flat, thin, reflective surface panels to a parabolic substructure as shown in Fig. 1. In a previous report [1], a study was made to predict the magnitude, direction and distribution of contact stresses required to hold the reflective surface (made of a single thin glass panel), after experiencing large displacements, to a rigid parabolic substructure. Particular attention was focussed on the edge effect occurring near each rim; that is, the appearance of localized contact stresses of higher magnitude than those acting on the rest of the panel, and a corresponding deviation from the true parabolic shape. The edge effect resulted from the absence of mechanical loads at the rim which were otherwise required to maintain the nonzero curvature defined by the true parabolic shape. By forming the reflective surface with two panels, additional free edges are created at the vertex. Consequently, a second edge effect region appears, though its presence does not affect the results obtained for the rim. In this report, a study of the vertex edge effect is presented. The results again show a localized contact stress variation and a loss of the true parabolic shape at the vertex similar to that occurring at the rim, but of greater magnitude. In addition, the analysis predicts a localized shear distribution on the back surface of the reflective panel.

ANALYSIS

In Fig. 2, one of the reflective panels is shown with the loads necessary to maintain the parabolic shape defined by

$$y = \frac{x^2}{4f} , \quad (1)$$

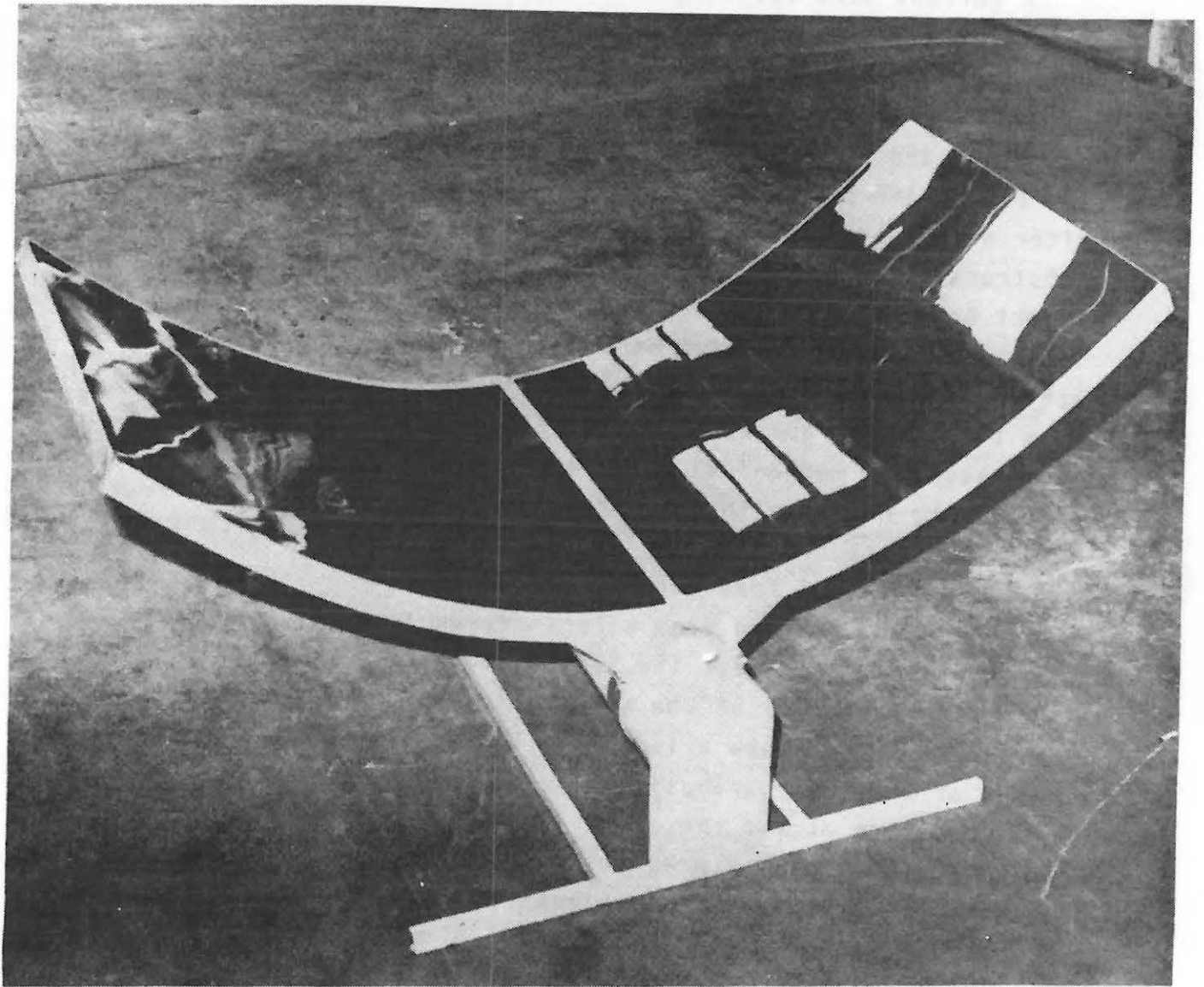


FIGURE 1. Assembled, parabolic, line focusing solar collector.

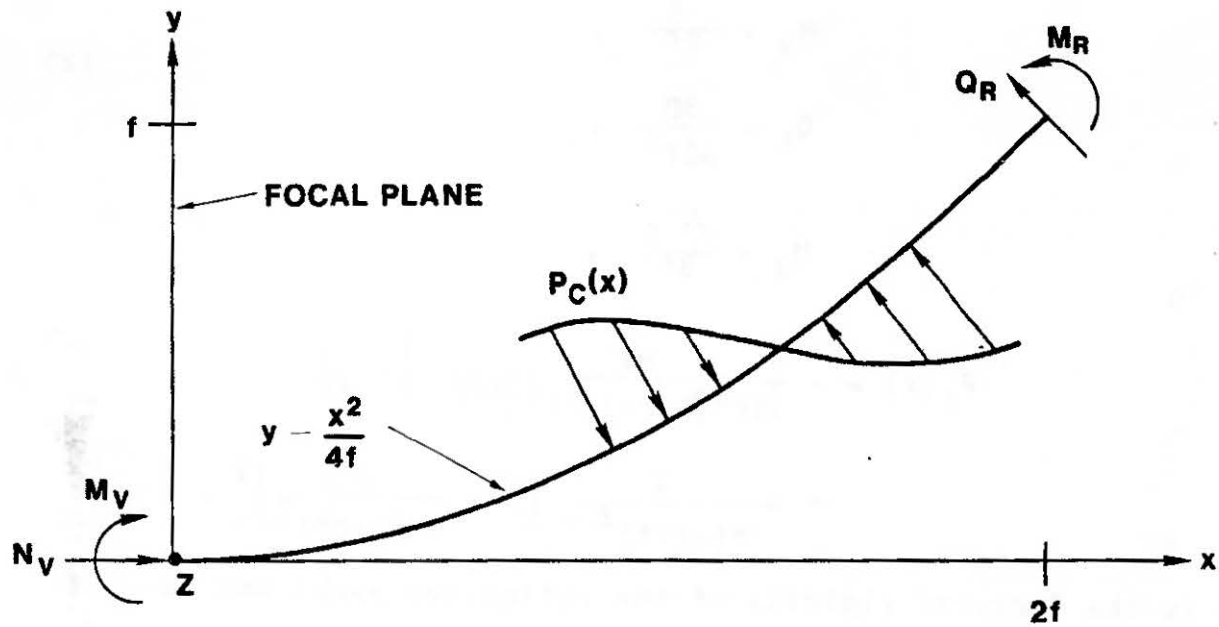


FIGURE 2. Diagram of half of the deformed, reflective surface explicating coordinates, rim and vertex loads and pressure distribution required to achieve the true parabolic shape.

where f is the focal length of the parabola. The loads shown in the figure have been calculated in [1] and are summarized below:

$$\begin{aligned}
 N_V &= \frac{7D}{64f^2} \quad , \\
 M_V &= \frac{D}{2f} \quad , \\
 Q_R &= \frac{3D}{32f^2} \quad , \\
 M_R &= \frac{\sqrt{2} D}{8f} \quad ,
 \end{aligned}
 \tag{2}$$

$$\begin{aligned}
 P_C(x) &= - \frac{5D}{16f^3 [1+(x/2f)^2]^{3/2}} \left\{ - \frac{1}{40} \right. \\
 &\quad \left. + \frac{1}{1+(x/2f)^2} \left(6 - \frac{7}{1+(x/2f)^2} \right) \right\} .
 \end{aligned}$$

D is the flexural rigidity of the reflective panel and is defined by

$$D = \frac{E_p h_p^3}{12(1-\nu^2)} \quad ,$$

where E_p is Young's modulus, ν is Poisson's ratio and h_p is the panel thickness. In [1] the residual loads at the rim, M_R and Q_R , were removed to satisfy the actual free edge conditions, and were replaced by equivalent normal tractions (contact stresses) applied to the back surface of the reflective panel and localized near the rim. This equivalent stress distribution, $\sigma_R(x)$, defined by

$$\sigma_R(x) = - \frac{\beta^3 D}{16(\beta f)^2} e^{-\beta(2f-x)} \left[(3+4\sqrt{2}(\beta f)) \cos\beta(2f-x) - 4\sqrt{2}(\beta f) \sin\beta(2f-x) \right] , \tag{3}$$

was shown to occur within a distance, δ_2 , (referred to as the second cross-over distance) from the rim. It was possible to relate this distance to the material properties of the substructure through the relationship

$$\delta_2 = \frac{5\pi}{4\beta} \quad (4)$$

where

$$\beta = \sqrt[4]{\frac{k}{4D}} \quad (5)$$

Expression (4) is an approximation of

$$\beta - \beta \tan \beta(2f-x) + \frac{Q_R}{M_R} = 0, \quad (6)$$

which defines the zeros of displacement or normal stress near the rim. To obtain (4), the quantity Q_R/M_R was neglected in comparison to β , based on the focal lengths of interest. In addition to introducing the stress distribution, removal of the rim loads resulted in a loss of the true parabolic shape. This loss was characterized by the rotation of the surface normals (slope error) defined by

$$w_R'(x) = \frac{1}{64(\beta f)^2} e^{-\beta(2f-x)} \left[(3+8\sqrt{2}(\beta f)) \cos \beta(2f-x) - 3\sin \beta(2f-x) \right]. \quad (7)$$

The expressions characterizing the stress distribution, σ_R , and the slope error, w_R' , are shown graphically in Figs. 3 and 4 for various values of δ_2 .

For the analysis of the two panel, or half parabola design the free edge at the vertex requires the removal of the vertex

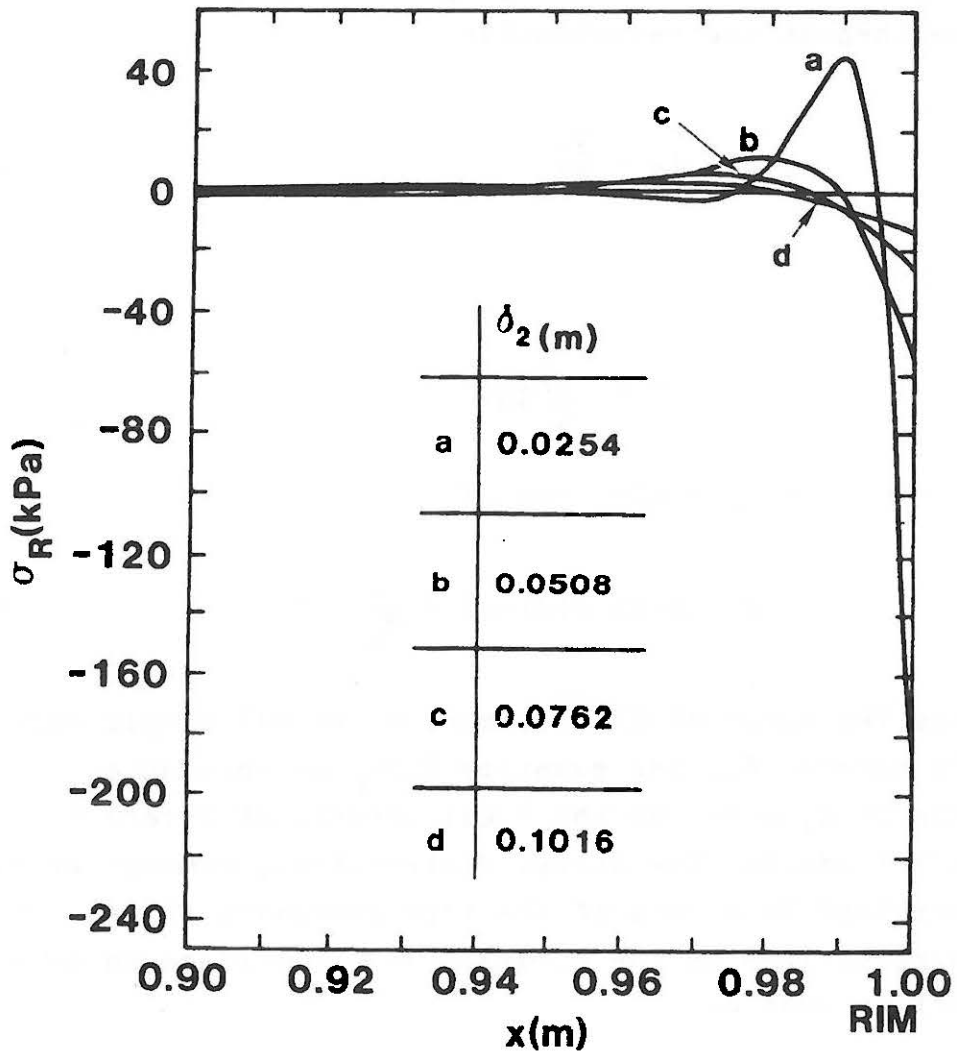


FIGURE 3. Contact stresses in adhesive applied to backside of deformed reflective surface arising from edge effect at rim.

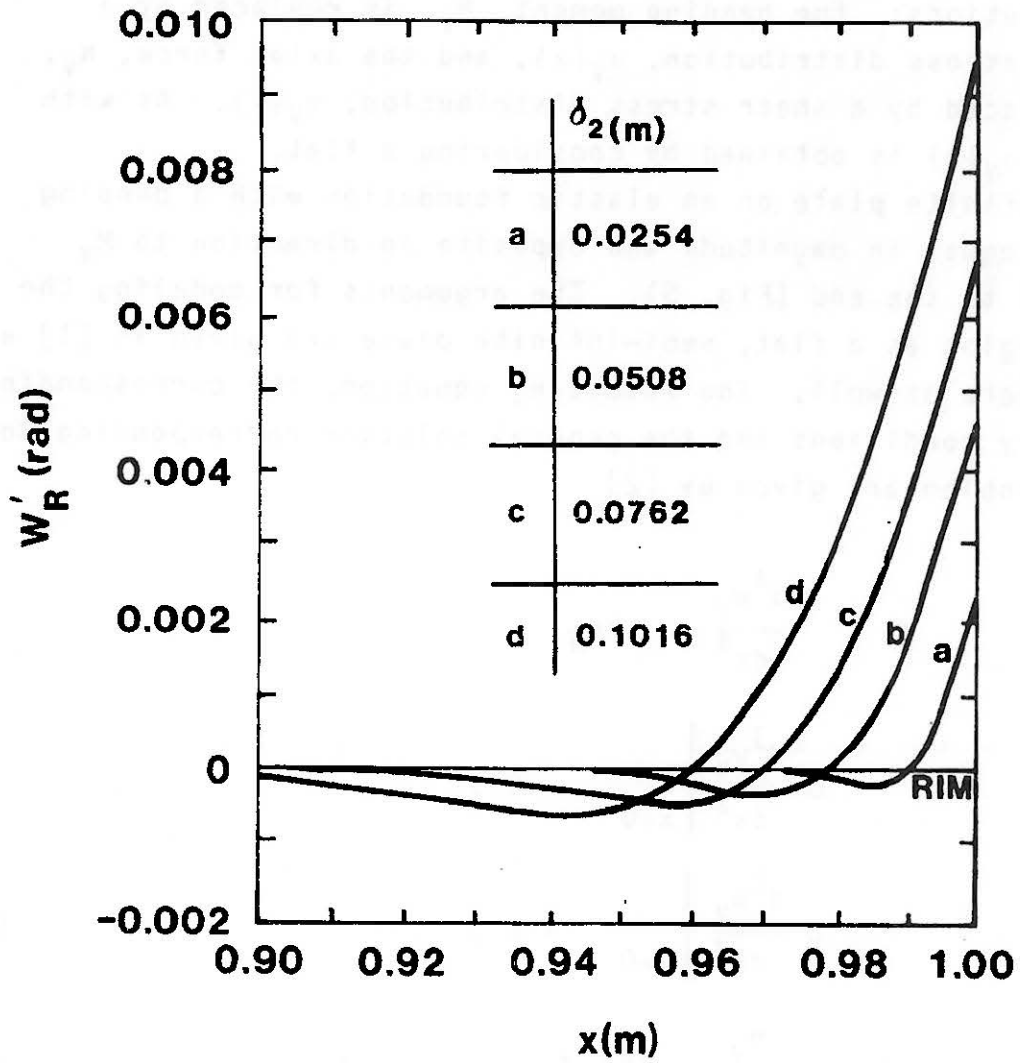


FIGURE 4. Rotation of surface normals (slope error) arising from edge effect at rim.

loads, N_V and M_V , to satisfy the actual boundary conditions. As in [1], they are replaced by equivalent stress distributions: the bending moment, M_V , is replaced by a normal stress distribution, $\sigma_V(x)$, and the axial force, N_V , is replaced by a shear stress distribution, $\tau_V(x)$. As with $\sigma_R(x)$, $\sigma_V(x)$ is obtained by considering a flat, semi-infinite plate on an elastic foundation with a bending moment equal in magnitude and opposite in direction to M_V applied to the end (Fig. 5). The arguments for modeling the edge region as a flat, semi-infinite plate are given in [1] and apply here as well. The resulting equation, the corresponding boundary conditions and the general solution corresponding to this problem are given by [2]

$$\frac{d^4 w_V}{dx^4} = -kw_V \quad , \quad (8)$$

$$D \left. \frac{d^3 w_V}{dx^3} \right|_{x=0} = 0 \quad , \quad (9)$$

$$D \left. \frac{d^2 w_V}{dx^2} \right|_{x=0} = 0 \quad , \quad (10)$$

$$w_V(x) = \frac{M_V}{2\beta^2 D} e^{-\beta x} [\sin \beta x - \cos \beta x] \quad . \quad (11)$$

Computing the corresponding tension in the foundation gives the normal stress distribution in the adhesive, namely

$$\sigma_V(x) = kw_V(x) = 2M_V \beta^2 e^{-\beta x} [\sin \beta x - \cos \beta x] \quad . \quad (12)$$

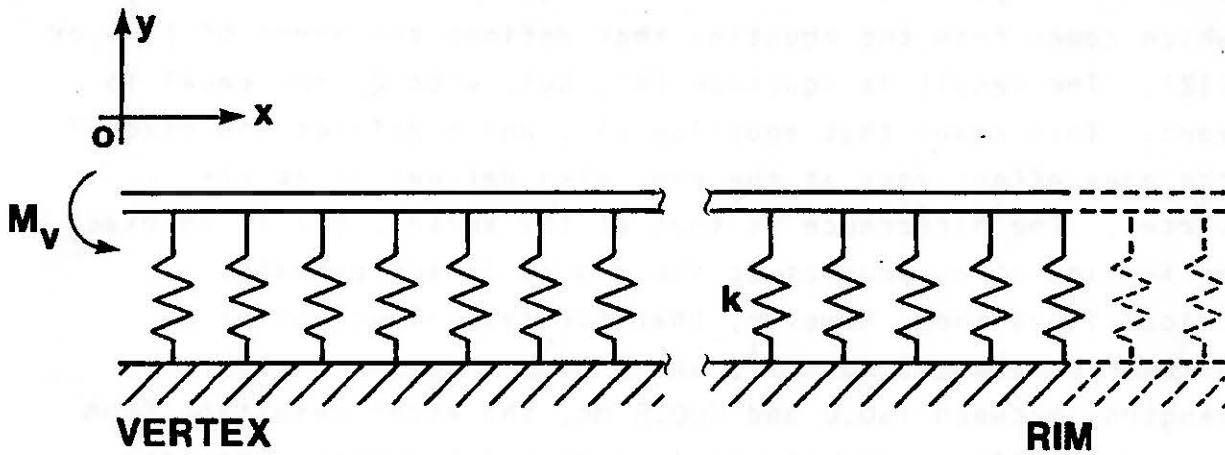


FIGURE 5. Diagram of the flat-plate model of the edge effect region at vertex explicating the coordinate system and semi-infinite extension.

Differentiating w with respect to x gives an expression for the slope error in the form

$$w'_V(x) = \frac{M_V}{\beta D} e^{-\beta x} \cos \beta x \quad . \quad (13)$$

General observations and optical measurements [4] of completed collectors suggest that the size of the edge effect zone at the vertex is approximately the same as it is at the rim. The present analysis verifies this through the definition of δ_2 which comes from the equation that defines the zeros of (11) or (12). The result is equation (6), but, with Q_R set equal to zero. This means that equation (4), which defines the size of the edge effect zone at the rim, also defines it at the vertex. The difference is that at the vertex, (4) is an exact definition of δ_2 whereas at the rim it is approximate. Calculations show, however, that for typical values of β , between 1.96 and 7.85 mm^{-1} , and a wide range of focal lengths, between 150.0 and 900.0 mm , the error resulting from the use of (4) at the rim is less than 3.0 percent (for the value of $f = 480.8 \text{ mm}$ used in the actual collector the error is less than 1.0 percent). On this basis, the present analysis predicts that the size of the edge effect zone, given by (4), is approximately the same at both the rim and the vertex, provided the values of the substructure stiffness (and hence the value of β) is also the same. Typical values of δ_2 are shown in Table 1 along with the corresponding stiffness, k_g , of the elastic foundation representing the adhesive plus the substructure. As in [1], a glass plate of thickness $h_p = 1.27 \text{ mm}$, Young's Modulus $E_p = 70 \text{ GPa}$ and Poisson's ratio $\nu = 0.24$ (yielding $D = 12.5 \text{ N-m}$) was used in the calculations of k . In Figs. 6 and 7, the stresses and slope errors in the vertex edge zone are plotted for the data in Table 1.

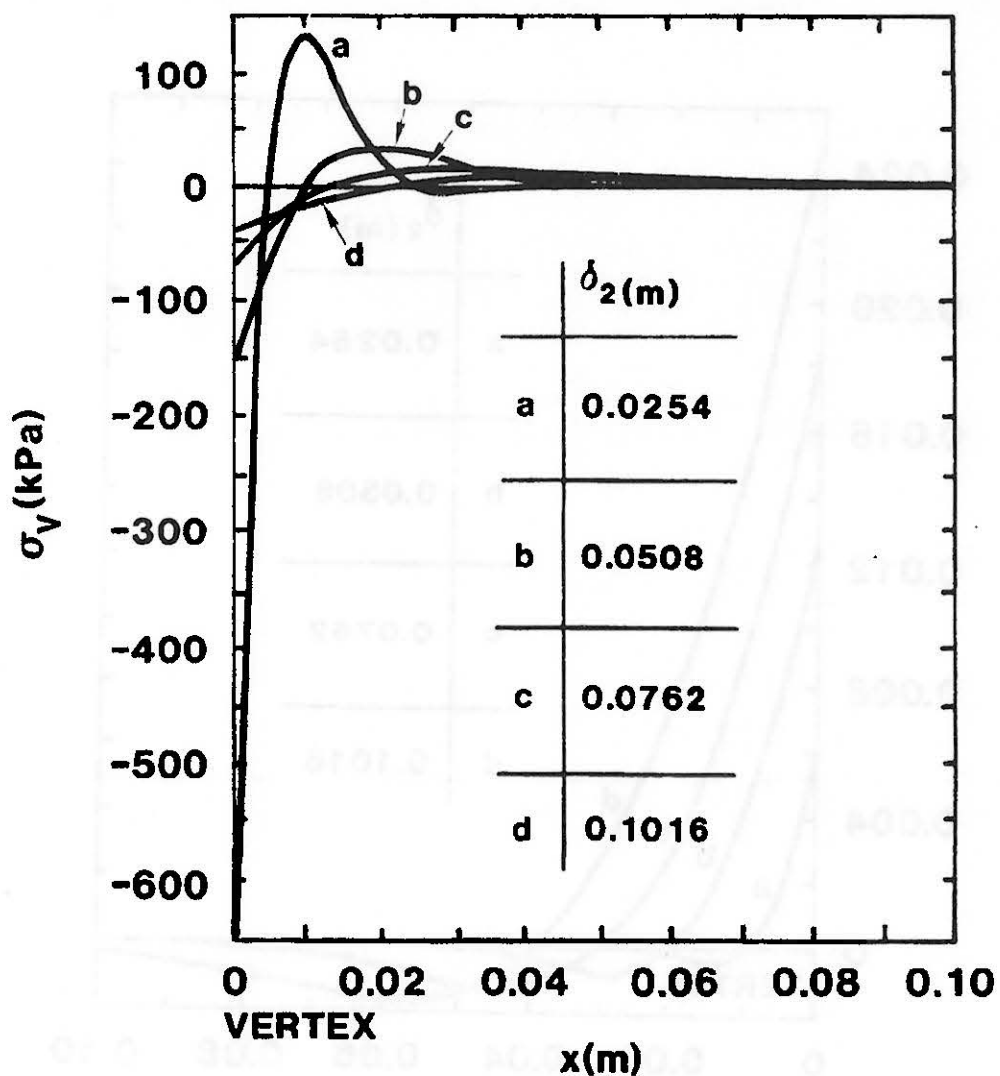


FIGURE 6. Contact stresses in adhesive applied to backside of deformed reflective surface arising from edge effect at vertex.

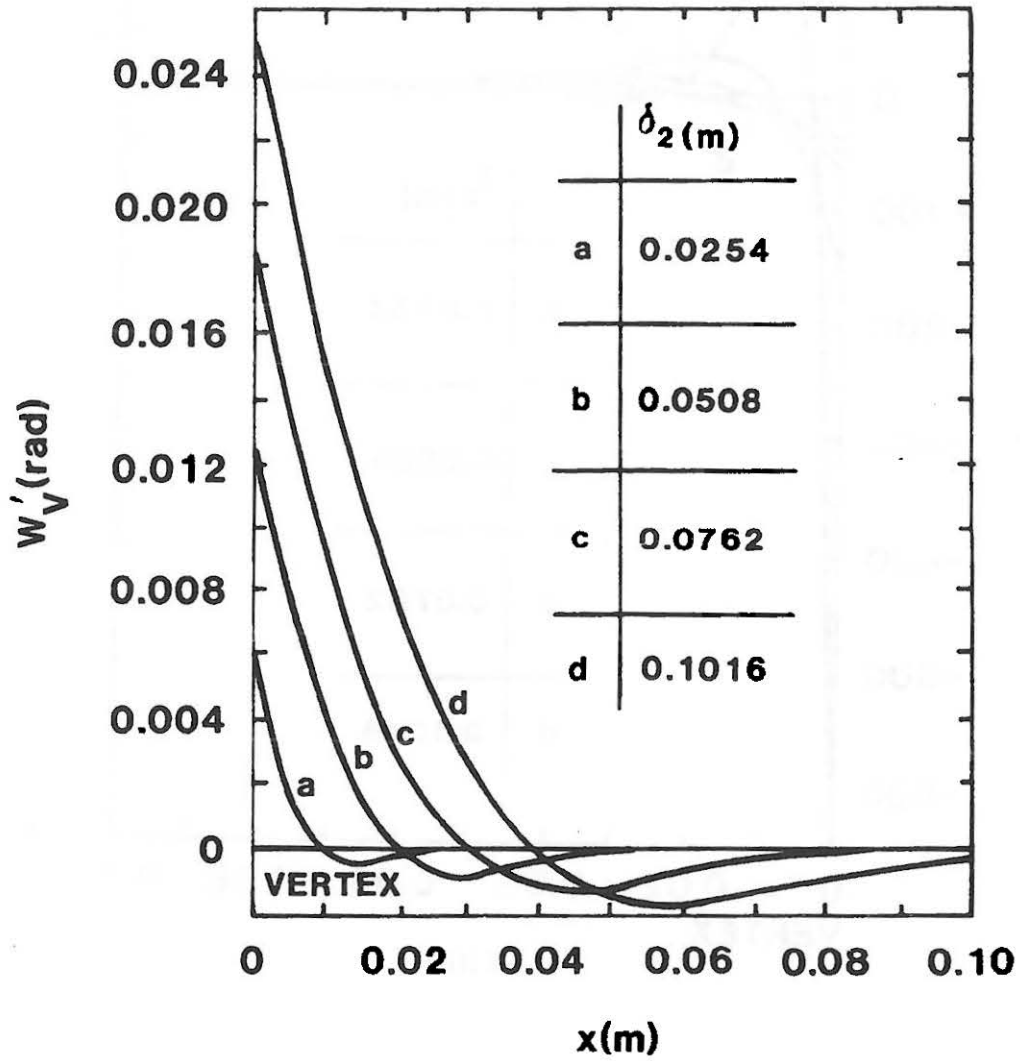


FIGURE 7. Rotation of surface normals (slope error) arising from edge effect at vertex.

TABLE 1
Edge Effect Parameters

| | | | | | |
|-----------------|-------------------|---------------------|---------------------|---------------------|---------------------|
| $\delta_2(m)$ | 0.0127 | 0.0254 | 0.0508 | 0.0762 | 0.1016 |
| $\beta(m^{-1})$ | 308.4 | 154.61 | 77.3 | 51.5 | 38.6 |
| $k(N-m)$ | 1.900×10 | 1.188×10^5 | 7.426×10^2 | 1.467×10^2 | 4.639×10^1 |

To determine the shear stress distribution, $\tau_v(x)$, consider a flat, semi-infinite plate resting on an elastic layer with a force, equal in magnitude and opposite in direction to N_v , applied to the plate at the vertex (Fig. 6). The equation for determining the shear stress in the adhesive is given by [3] as

$$\frac{d^2 \tau_v}{dx^2} - 4\gamma^2 \tau_v = 0, \quad (14)$$

where

$$\gamma^2 = \frac{G_a}{4E_p h_p h_a}. \quad (15)$$

In (15), G_a is the shear modulus of the adhesive and h_a is its thickness. The boundary conditions associated with (14) are

$$\tau_v(x) \Big|_{x=2f} = 0, \quad (16)$$

$$\int_0^{2f} \tau_v(x) dx = N_v, \quad (17)$$

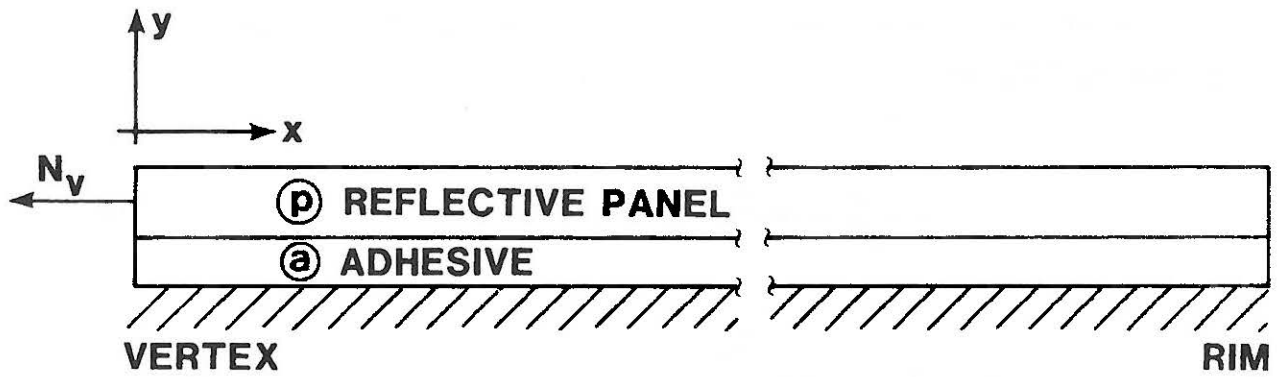


FIGURE 8. Diagram of the flat plate model used to analyze shear deformation arising from edge effect at vertex.

where (17) is the equation for equilibrium in the x direction. The solution to (14), subject to (16) and (17), is given by

$$\tau_v(x) = \frac{2\gamma N_v}{\cosh 4\gamma f - 1} [\sinh(4\gamma f) \cosh(2\gamma x) - \cosh(4\gamma f) \sinh(2\gamma x)]. \quad (18)$$

By noting that for focal lengths of interest $\cosh 4\gamma f \gg 1$ and $\tanh 4\gamma f \approx 1$, (18) can be simplified to read

$$\tau_v(x) \approx 2\gamma N_v [\cosh 2\gamma x - \sinh 2\gamma x]. \quad (19)$$

In Table 2 are some typical values of the plate and adhesive properties, with the corresponding shear stress distributions shown in Fig. 9.

TABLE 2
Typical Values of Panel and Adhesive Properties

| | CASE I | CASE II | CASE III |
|------------|------------------------|------------------------|------------------------|
| E_p (Pa) | 6.895×10^{10} | 6.895×10^{10} | 6.895×10^{10} |
| ν | .240 | .240 | .240 |
| h_p (mm) | 0.76 | 1.27 | 1.27 |
| h_a (mm) | 0.5 | 0.5 | 0.38 |
| G_a (Pa) | 2.068×10^8 | 2.068×10^8 | 2.068×10^9 |

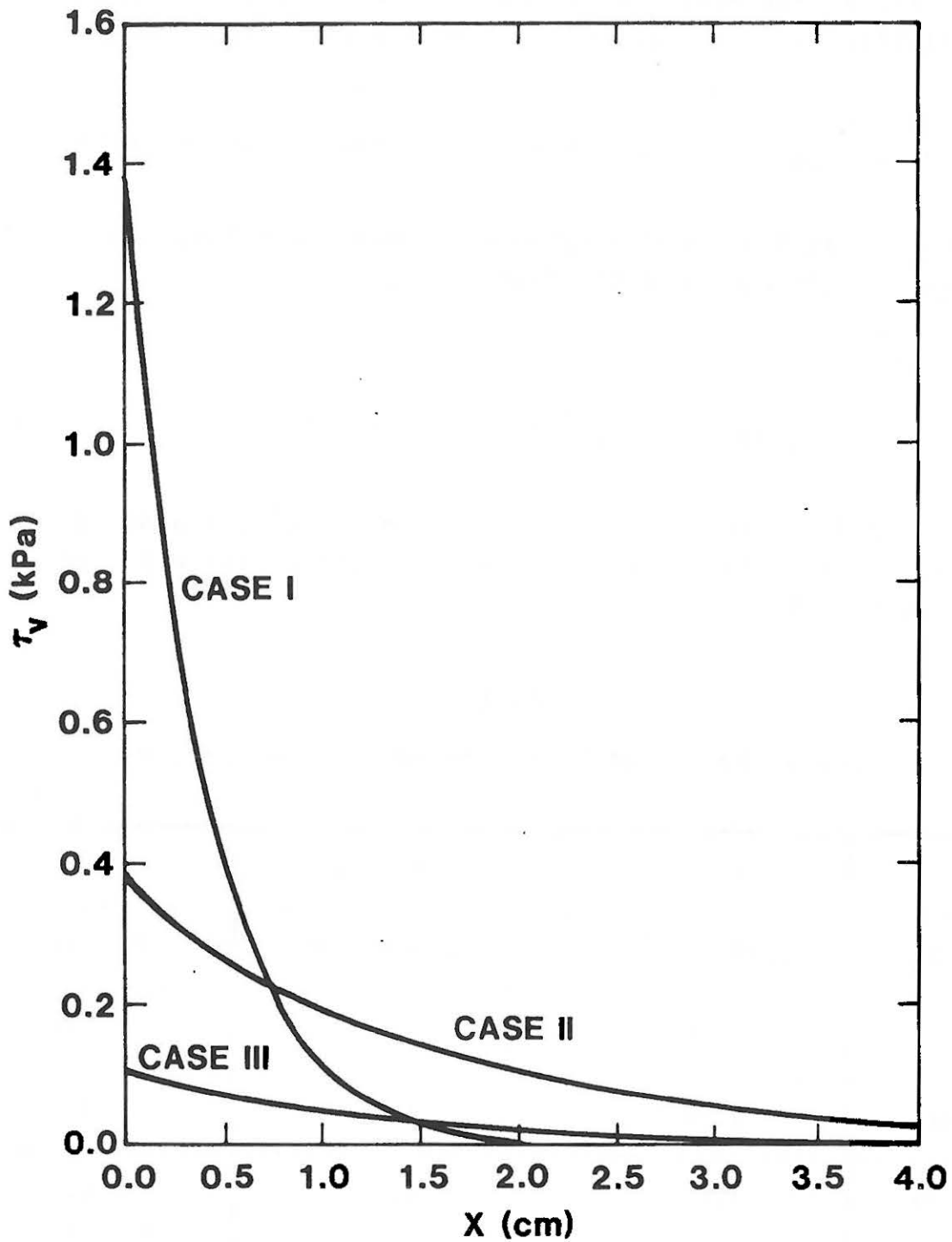


FIGURE 9. Shear stresses in adhesive applied to backside of deformed reflective surface arising from edge effect at vertex.

DISCUSSION OF RESULTS

The curves showing the normal stress distribution and slope errors in the edge effect region near the vertex, Figs. 6 and 7, can be compared with the corresponding curves for the edge effect at the rim, Figs. 3 and 4, to show that the effect is more pronounced at the vertex. Stress levels at the vertex are approximately twice those at the rim and, similarly, the maximum slope error is approximately two times larger at the vertex. However, since the distance from the vertex to the focal line, f , is half the distance from the rim to the focal line, $2f$, the distance by which the reflected rays from the two locations miss the focal line, $w'f$, is approximately the same. The significance of the higher slope errors at the vertex is further mitigated by virtue of receiver tube shadowing. Because of the large stresses in the edge effect zone near the vertex, however, any delamination problems would be expected to occur there first. Maximum tensile stresses occur slightly away from the vertex edge (between δ_1 and δ_2), Fig. 6, and it is conceivable that a delamination initiated there would arrest itself, creating significantly greater slope errors in the process. The delamination would grow away from the vertex because of the compressive stresses which will always reside at the edge, and an arrest would take place when the delamination grew to a size representative of a large enough edge effect zone to reduce stresses sufficiently.

Laser ray tracings showing slope errors are plotted in Figs. 10 and 11 to emphasize the agreement between the above results and experiment. Not only are the edge effects at the vertex and rim clearly defined but the difference in the magnitudes of the slope errors in the two locations are also evident. In Fig. 12, data from Fig. 11 has been superimposed on the analytical results to show the correlation between theory and experiment. It is emphasized here that this correlation is only in regard to the edge effect. Away from the free ends of

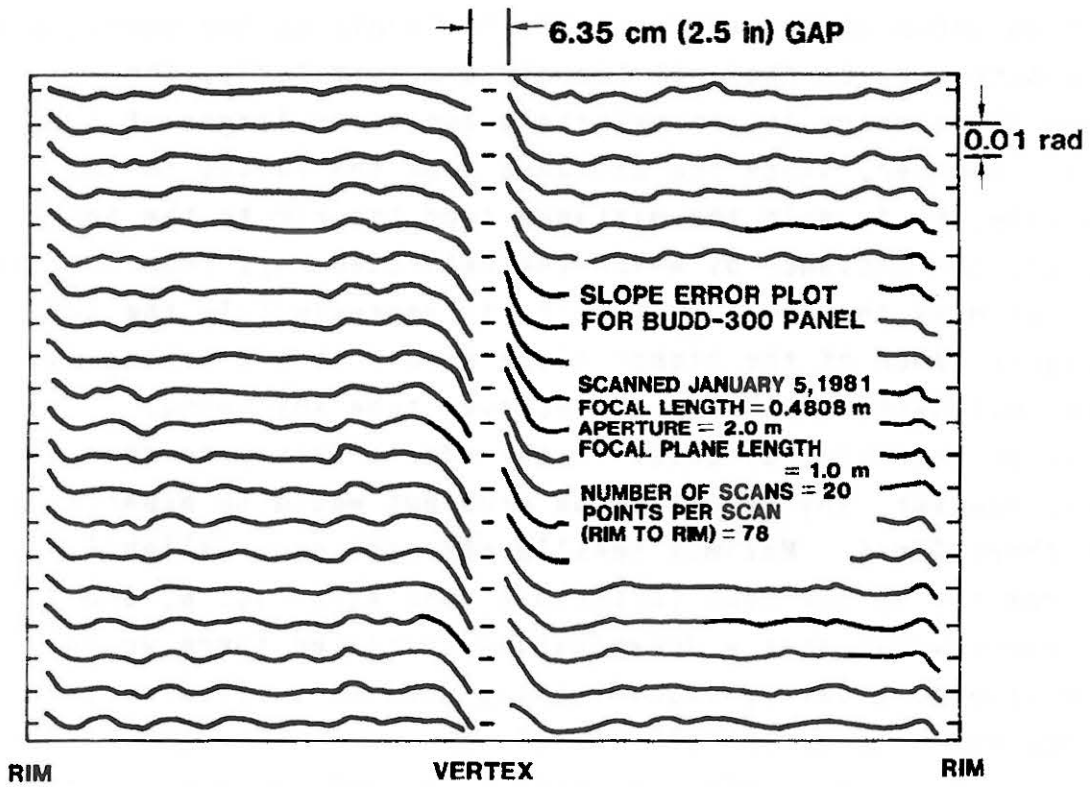


FIGURE 10. Typical results from laser ray tracing showing slope errors at rim and vertex.

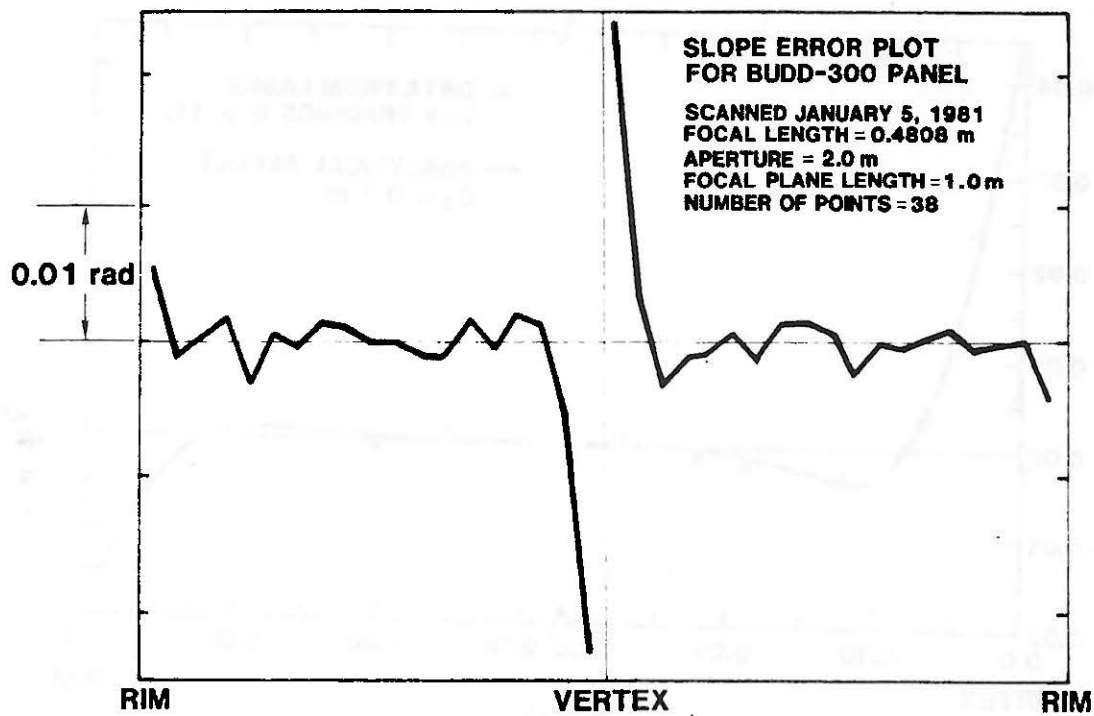


FIGURE 11. Single scan taken from laser ray tracing showing slope errors at rim and vertex.

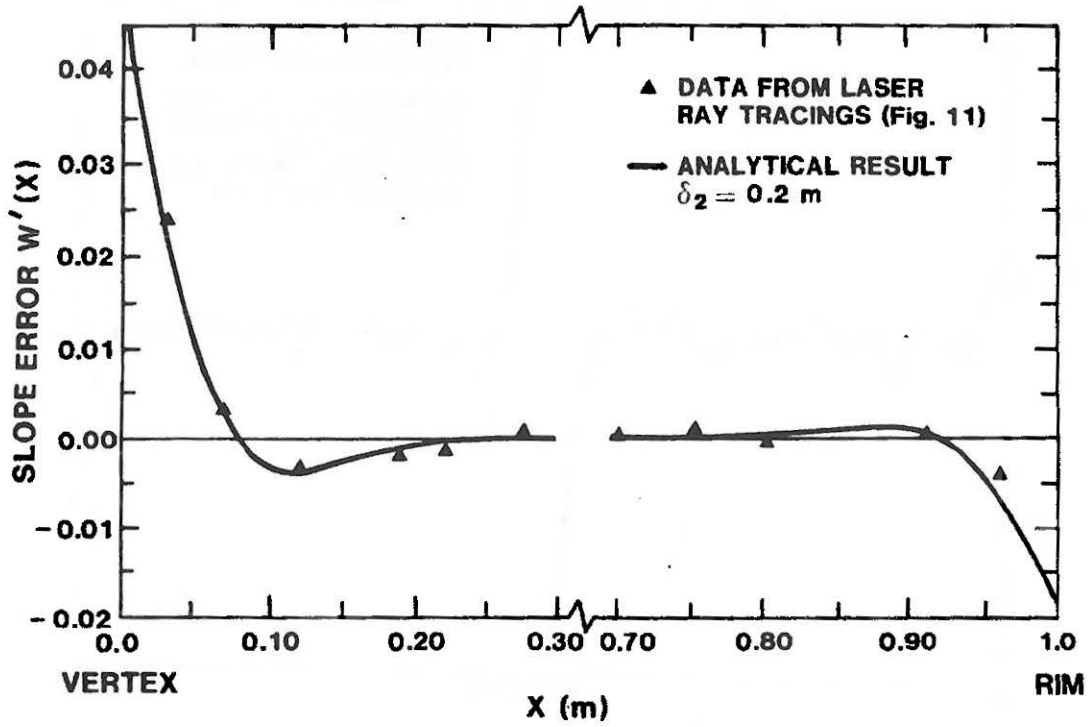


FIGURE 12. Correlation between analytical results [eqs (7) and (13)] and laser ray tracing data (Fig. 11).

the collector, anomalies associated with the substructure introduce additional effects, though relatively small, which are shown in the experimental results (Figs. 11 and 12) but which are not introduced into the analytical model.

Finally, a glance at Fig. 9 shows that the consequences of shear stress due to edge effects are negligible, even for the weakest of back surface coatings or adhesives.

REFERENCES

1. Reuter, R. C., Jr., and Wilson, R. K., "Contact Stresses on a Thin Plate After Large Displacements to a Full Parabolic Surface," Sandia National Laboratories, Report No. SAND81-2083 (1981).
2. Boresi, A. P., Sidebottom, O. M., Seely, F. B., and Smith, J. O., Advanced Mechanics of Materials, 3rd Edition, John Wiley & Sons, NY, NY (1978).
3. Goland, M. and Reissner, E., "The Stresses in Cemented Joints," J. Appl. Mech., Trans. ASME 66, A-17 (1944).
4. Hansche, B. D., "Laser Ray Trace Testor for Parabolic Solar Collectors," Instrum. Soc. of Am. Proceedings, Vol. 19, No. 2, p. 43 (1980).



NTIS does not permit return of items for credit or refund. A replacement will be provided if an error is made in filling your order, if the item was received in damaged condition, or if the item is defective.

Reproduced by NTIS

National Technical Information Service
Springfield, VA 22161

*This report was printed specifically for your order
from nearly 3 million titles available in our collection.*

For economy and efficiency, NTIS does not maintain stock of its vast collection of technical reports. Rather, most documents are printed for each order. Documents that are not in electronic format are reproduced from master archival copies and are the best possible reproductions available. If you have any questions concerning this document or any order you have placed with NTIS, please call our Customer Service Department at (703) 605-6050.

About NTIS

NTIS collects scientific, technical, engineering, and business related information — then organizes, maintains, and disseminates that information in a variety of formats — from microfiche to online services. The NTIS collection of nearly 3 million titles includes reports describing research conducted or sponsored by federal agencies and their contractors; statistical and business information; U.S. military publications; multimedia/training products; computer software and electronic databases developed by federal agencies; training tools; and technical reports prepared by research organizations worldwide. Approximately 100,000 *new* titles are added and indexed into the NTIS collection annually.

For more information about NTIS products and services, call NTIS at 1-800-553-NTIS (6847) or (703) 605-6000 and request the free *NTIS Products Catalog*, PR-827LPG, or visit the NTIS Web site <http://www.ntis.gov>.

NTIS

*Your indispensable resource for government-sponsored
information—U.S. and worldwide*

Reproduced by NTIS

National Technical Information Service



U.S. DEPARTMENT OF COMMERCE
Technology Administration
National Technical Information Service
Springfield, VA 22161 (703) 605-6000



DE82006998



BA

BIN: M38 01-25-02
INVOICE: 1128512
SHIPTO: 1*16322
PAYMENT: CSH*V